RESEARCH ARTICLE

Subcellular proteomics revealed the epithelial–mesenchymal transition phenotype in lung cancer

Li-Ping Li[1], Chun-Hua Lu[1,2]*, Zhi-Peng Chen[1]*, Feng Ge[1], Tong Wang[1], Wei Wang[3], Chuan-Le Xiao[1], Xin-Feng Yin[1], Langxia Liu[1], Jian-Xing He[3]** and Qing-Yu He[1]*

[1] Institute of Life and Health Engineering/National Engineering and Research Center for Genetic Medicine, Jinan University, Guangzhou, P. R. China
[2] College of Life Science and Technology, Guangxi University, Nanning, P. R. China
[3] State Key Laboratory of Respiratory Disease, First Affiliated Hospital of Guangzhou Medical College, Guangzhou, P. R. China

Received: December 12, 2009
Revised: November 10, 2010
Accepted: November 10, 2010

Subcellular proteomics was used to compare the protein profiles between human lung adenocarcinoma A549 cells and human bronchial epithelial (HBE) cells. In total, 106 differential proteins were identified and the altered expression levels of partial identified proteins were confirmed by Western blot analysis. Importantly, pathway analysis and biological validation revealed epithelial–mesenchymal transition (EMT) phenotype shift in A549 cells as compared with HBE cells. The EMT phenotype of A549 cells can be increased by self-producing TGF-β1 and significantly decreased by silencing heterogeneous nuclear ribonucleoprotein (hnRNPK) expression. As EMT has been considered as an important event during malignant tumor progression and metastasis, investigating EMT and deciphering the related pathways may lead to more efficient strategies to fight lung cancer progression. By integrating the subcellular proteomic data with EMT-related functional studies, we revealed new insights into the EMT progress of lung carcinogenesis, providing clues for further investigations on the discovery of potential therapeutic targets.

Keywords:
Cell biology / Epithelial-mesenchymal transition / Heterogeneous nuclear ribonucleoprotein K / Lung cancer / Subcellular proteomics

1 Introduction

Lung cancer represents one of the most debilitating malignancies, accounting for ~25% of all cancer deaths worldwide [1]. Regardless of subtypes, the 5-year survival rate for lung cancer is among the lowest of all cancers [2]. Because of the nodal or distant metastasis in lung cancer, the risk of recurrence cannot be reduced even complete surgical resection is performed [3]. Metastasis of lung cancer cells is one of the major reasons for the low survival rate. The progress of metastasis includes the cell detachment from primary tumor, invasion to extracellular matrix and spread

Correspondence: Professor Qing-Yu He, Institute of Life and Health Engineering/National Engineering and Research Center for Genetic Medicine, Jinan University, Guangzhou 510632, P. R. China
E-mail: tqyhe@jnu.edu.cn; heqy1@yahoo.com
Fax: +86-20-85227039 I

Abbreviations: Ab, antibody; **DEP,** differentially expressed protein; **EMT,** epithelial–mesenchymal transition; **GPX1,** glutathione peroxidase 1; **HBE,** human bronchial epithelial; **hnRNP,** heterogeneous nuclear ribonucleoprotein; **KRT,** cytokeratin; **siRNA,** small interfering RNA; **VCL,** vinculin

*These authors have contributed equally to this work.

**Additional corresponding author: Professor Jian-Xing He, E-mail: hejx@vip.163.com

Colour Online: See the article online to view Figs. 3 and 8 in colour.

with blood vessels [4]. The process of detachment is a prerequisite for the metastasis, which is accompanied by the loss of adherent junctions and tight junctions, and cytoskeletal reorganization.

Epithelial–mesenchymal transition (EMT) is a process of malignant transition that leads to enhanced carcinoma metastasis [5]. In EMT, cells lose their epithelial characteristics such as cell polarity, cell–cell contact, and gain mesenchymal properties, and thus EMT is a crucial event for cancer cells to acquire invasive and metastatic phenotypes [6, 7]. Although EMT has been widely investigated [8–13], detailed mechanisms of its occurrence in cancer cells, especially in lung cancer cells, are not fully understood.

In the present study, we used 2-DE coupled with subcellular fractionation to compare the differences in protein expression between lung cancer cell line A549 and human bronchial epithelial (HBE) cells. Many proteins related to EMT were found to have different expressions in cancer cells. Further functional studies confirmed the shift of the EMT phenotype in A549 cells. The current findings provide not only insights into the mechanism underlying lung carcinogenesis but also direct implications for the development of novel therapeutic strategies.

2 Materials and methods

2.1 Cell culture

The HBE and A549 cells (human lung adenocarcinoma) were purchased from American Type Culture Collections (ATCC, Rockville, MD, USA). The cells were maintained in 75-cm^2 culture flasks in RPMI 1640 culture medium (Invitrogen, Carlsbad, CA, USA) supplemented with 10% FBS (Hyclone, Waltham, MA, USA), 1% penicillin/streptomycin in a CO_2 incubator (5% CO_2:95% air) at 37°C. After growth to confluence, the cells were detached with a 0.25% trypsin/0.02% EDTA solution for passage.

2.2 Cell fractionation

Subcellular proteins were extracted by using Fraction PREP™ cell fractionation system (BioVision, Mountain View, CA, USA) according to the manufacturer's instructions. Briefly, four subcellular protein fractions including cytosolic, membrane/organelles, nucleic, and cytoskeleton proteins were acquired by treating cell lysates with the fraction-specific buffers provided in the kit. Protein fractions were purified by ice-cold acetone and dissolved in 2-DE lysis buffer as described previously [14]. Protein concentration was determined by protein assays (BioRad, Richmond, CA, USA).

2.3 2-DE and image analysis

The detailed materials and methods of 2-DE had been described previously [14]. Briefly, each sample containing 150 μg proteins in 250 μL of rehydration solution was isoelectrically separated on a 13-cm immobilized pH 3–10 nonlinear IPG strip. Secondary protein separation was then performed with 12.5% SDS-PAGE gel, followed by silver-staining visualization and image acquisition. Gel images were analyzed with ImageMaster 2D Platinum 6.0 (GE Healthcare, Uppsala, Sweden). The spots with significant differences at fold change over 1.5 across three analytical gels were picked and subjected to tryptic digestion and mass spectrometric (MS) analysis.

2.4 Tryptic in-gel digestion and MALDI-TOF/TOF MS analysis

The protein spots with significant differences were excised for tryptic in-gel digestion as described previously [15]. The digested peptides were analyzed on an ABI 4800-plus MALDI TOF/TOF mass spectrometer (Applied Biosystems, Foster City, CA, USA). The MS and MS/MS data were interpreted using GPS Explorer software (V3.6, Applied Biosystems) and submitted to MASCOT search engine (V2.1, Matrix Science, London, UK) [14] for protein identification.

2.5 Bioinformatics

Differentially expressed proteins (DEPs) were classified based on the PANTHER (Protein ANalysis THrough Evolutionary Relationships) system (http://www.pantherdb.org) [16, 17]. DEPs were further analyzed by Ingenuity pathways analysis (Ingenuity Pathway® Analysis, IPA, Ingenuity Systems, www.Ingenuity.com) [18, 19]. Briefly, the fold changes of DEPs were uploaded into IPA system with gene identifier. With core analysis module, IPA generated computational networks that are biologically relevant to particular functions. The significance (*p*-values) given showed the correlation between the data uploaded and the canonical pathway stored in the IPA knowledge base.

The pathway network constructed by IPA is a graphical representation of the cellular assembly and organization. Solid lines and broken lines indicate direct and indirect interactions, respectively. The single line connection means binding interaction, whereas lines with arrowheads indicate ''act upon''. For the shapes, ovals stand for transcription regulators, diamonds for enzymes, squares for cytokines, rectangles for ligand-dependant nuclear factors, triangles for kinases, trapezoids for transporters, and circles for others. Pink-color nodes represent upregulation, whereas green ones stand for downregulated proteins in A549. Deeper color means greater regulation. Nodes without color

represent proteins with their input depending on the IPA analysis.

2.6 Western blotting analysis

Protein extracts were separated by 10% SDS-PAGE gels and transferred onto Immobilon-P PVDF transfer membranes (Millipore, Bedford, MA, USA). After being blocked by 5% nonfat milk, the membranes were incubated with primary antibodies (Abs), secondary Abs, followed by chemiluminescent visualization with SuperSignal West Pico kit (Pierce Biotechnology, Rockford, IL, USA). Primary Abs, if used, were diluted at 1:500 with primary Ab dilution buffer (PBST with 5% nonfat milk). These Abs included mouse anti-ZO-1 mAb (Becton-Dickinson, Heidelberg, Germany), rabbit anti-β-catenin mAb (Upstate Biotechnology, Waltham, MA, USA), rabbit anti-integrin β1 mAb, mouse anti-calpain 1 (CAPN1) mAb (Epitomics, Burlingame, CA, USA), mouse anti-Histone H1 mAb, mouse anti-vimentin mAb, mouse anti-cytokeratin 19 (KRT19) mAb, mouse anti-cytokeratin 18 (KRT18) mAb, rabbit anti-TOM40 polyclonal Ab, mouse anti-heterogeneous nuclear ribonucleoprotein (hnRNPK) mAb, goat anti-HSP27 polyclonal Ab, mouse anti-vinculin (VCL) mAb (all from Santa Cruz Biotechnology, Santa Cruz, CA, USA), rabbit anti-stathmin polyclonal Ab, rabbit anti-glutathione peroxidase 1 (GPX1) polyclonal Ab (Cell Signaling, Danvers, MA, USA), rabbit anti-E-cadherin polyclonal Ab, rabbit anti-*N*-cadherin polyclonal Ab (Abcam, Cambridge, MA, USA), and mouse anti-β-actin mAb (Proteintech Group, Chicago, IL, USA). Corresponding secondary Abs were also purchased from KPL, Gaithersburg, MD, USA.

2.7 Immunocytochemistry

A549 and HBE cells were cultured on sterile glass coverslips, and then fixed with 4% paraformaldehyde, permeabilized by 0.1% Triton X-100. After washing with PBS three times, slides were blocked with 5% sheep serum albumin for 1 h and then incubated with the rabbit anti-hnRNPK polyclonal Ab (Abcam), the rabbit anti-E-cadherin polyclonal Ab, and the mouse anti-vimentin polyclonal Ab (Cell Signal., Cambridge, MA, USA). All Abs were diluted at 1:500. For filamentous actin (F-actin) staining, the specimens were incubated with 0.25 μM Rhodamine-phalloidin (Sigma, Deisenhofen, Germany) in a humid chamber for 30 min at room temperature. After washing and incubating with Texas red-conjugated secondary Ab (Santa Cruz Biotechnology) for 1 h, the cells were incubated with DAPI (Sigma Chimie, St. Quentin Fallavier, France) for 15 min and washed again with PBS. The overslips were put on glass slides with antifade mounting regents and observed under Confocal Laser Miskcroscopy (Nikon, Japan). Pictures were captured using a Photometrics Coolsnap CF color camera (Nikon).

2.8 ELISA

The TGF-β1 level in supernatants of the two cell lines was measured by TGF-β1 enzyme-linked immunosorbent assay (ELISA) test kit (Dakewe, Shenzhen, China) according to the manufacturer's instruction. The experiments were repeated with triplicates in each test.

2.9 RNA interference

When cells reached 50% confluence in culture, RNA interference was performed. Briefly, the small interfering RNAs (siRNA) for hnRNPK or nontargeting siRNAs (100 nM) were intracellularly transfected using RNAiMAX (Invitrogen). The cells were then allowed to grow for another 48 h. hnRNPK siRNA was obtained from Shanghai GenePharma (GenePharma, Shanghai, China). hnRNPK siRNA1 (sense, 5′-GAUCAUCCUUGAUCUUAUATT-3′; antisense, 5′-UAUAAGAUCAAGGAUGAUCTT-3′), siRNA2 (sense, 5′-GGAUUCUAAUGCAAGAUAUTT-3′; antisense, 5′-AUAUCUUGCAUUAGAAUCCTT-3′) were chosen as the main siRNA with sufficient knockdown. All duplexes were dissolved to a final concentration of 20 μM and stored at −20°C.

2.10 Statistical analysis

Statistical analysis was performed using a Student's *t*-test when comparing two groups. Comparison between multiple groups was performed by one-way analysis of variance (ANOVA) with Bonferroni post-hoc *t*-test. Statistical calculation was performed by using SPSS 14.0 (SPSS, Chicago, IL, USA). Data were expressed as mean ± SD and significant difference was accepted at $p < 0.05$.

3 Results

3.1 Subcellular fractionation

To increase the resolution of 2-DE, A549 and HBE cells were subjected to subcellular fractionation prior to electrophoresis. SDS-PAGE and Western blotting were performed to evaluate the purity and enrichment efficiency of the fractionation. For this purpose, integrin β1, calpain, histone H1, and vimentin were employed as the purity controls for membrane/organelle, cytosolic, nuclear, and cytoskeletal protein fractions, respectively. SDS-PAGE images shown in Fig. 1A demonstrate that protein patterns of the respective fractions are clearly distinct; and the Western blotting

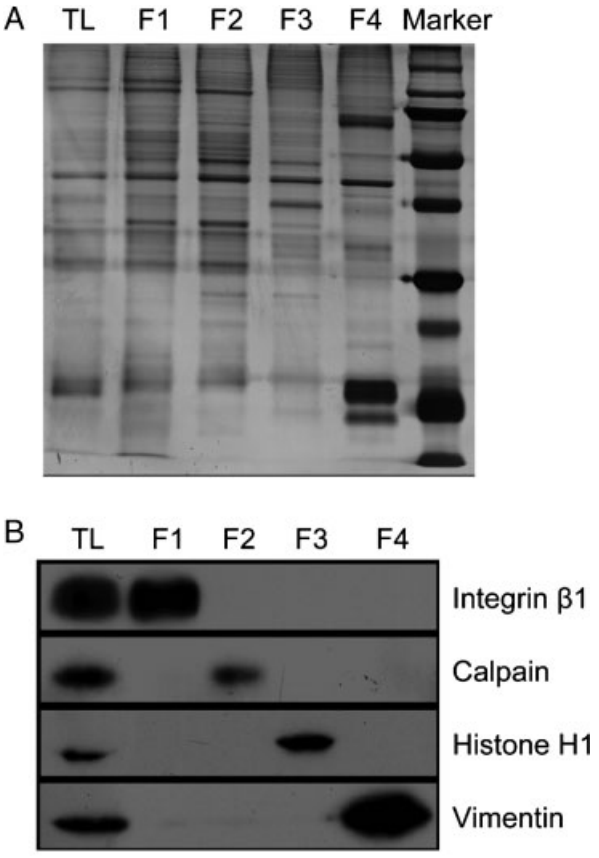

Figure 1. Subcellular protein extraction of A549. (A) SDS-PAGE of subcellular fractions, demonstrating that protein patterns of the respective fractions were clearly distinct. TL, total cell lysate; F1, membrane/organelle protein fraction; F2, cytosolic protein fraction; F3, nucleic protein fraction; and F4, cytoskeleton protein fraction. (B) Immunoblotting against marker proteins for each fraction, indicating that sufficiently pure and enriched subcellular fractions were obtained.

results in Fig. 1B indicate that sufficiently pure and enriched subcellular fractions were obtained, allowing us to proceed with 2-D PAGE analysis.

3.2 Subcellular proteome profiling of lung cells

The subcellular fractions of A549 and HBE cells were subjected to 2-DE proteomic profiling. Figure 2 shows the representative 2-DE proteomic maps of the nucleic fractions from A549 and HBE cells. Representative 2-DE maps of whole-cell proteins and other subcellular fractions are shown in Supporting Information figures. To obtain statistically significant results, each fraction sample was run in triplicate. Totally, 142 DEP spots were excised, in-gel digested by trypsin, and analyzed by MALDI-TOF/TOF MS. After eliminating redundant proteins, 106 DEPs were identified and are listed in Supporting Information Table S1.

3.3 Functional categorization and pathway analysis

The 106 identified proteins were categorized into 26 molecular functional groups and 26 biological processes according to PANTHER classification system (Fig. 3A and B). The majority of the identified proteins were found among protein species associated to nucleic acid binding (15.2%), oxidoreductase (12.1%), cytoskeletal protein (11.4%), regulatory molecule (7.6%), chaperone (6.1%), etc. It is feasible that the differential proteins identified in this study have a biological significance and thus may provide clues for understanding the molecular pathogenesis of lung cancer.

To identify the target pathways and proteins implicated by proteomic data acquired in this study, we performed a functional core analysis assisted by IPA. The complex proteomic data were abstracted and incorporated into a significant network of Cellular Assembly and Organization (scoring 56, p-value $= 2.89 \times 10^{-05}$–4.77×10^{-02}, Fig. 3C). Compared with those in HBE cells, actin-binding proteins including PDCD6IP, VCL, HSPB, and SCIN were all upregulated in A549 cells, promoting actin polymerization and stability. Moreover, KRT 17/18/19 were dramatically downregulated in A549 cells, indicating the occurrence of cytoskeleton reassembly. Interestingly, the hnRNP proteins including hnRNPD, hnRNPDL, and hnRNPK were integrated into this network by IPA system. The results of this pathway analysis suggested that A549 cells tend to have higher motility capacity than HBE cells. In conclusion from this analysis, A549 cells may be at a transition stage to mesenchymal phenotype (EMT transformation) and hnRNPK may play an important role in this network.

3.4 Confirmation of DEPs

To confirm the DEPs found in this study, we analyzed a panel of selected proteins by Western blotting, including KRT19, HSP27, TOM40, hnRNPK, CAPN1, GPX1, stathmin, and VCL. Relative intensity of these proteins was normalized to β-actin bands (Fig. 4). We observed the consistent alterations as obtained in 2-DE analysis, with the significantly decreased expressions of CAPN1, KRT18, KRT19, TOM40, and GPX1, and the substantially increased expressions of HSP27, hnRNPK, VCL, and stathmin in A549 cells.

3.5 Validation of differential subcellular distribution of hnRNPK

From the comparative subcellular proteomic analysis stated above, some proteins such as hnRNRK were found to have different expression alterations in different subcellular fractions. The alternative techniques of immunoblotting and immunofluorescence were employed to confirm the

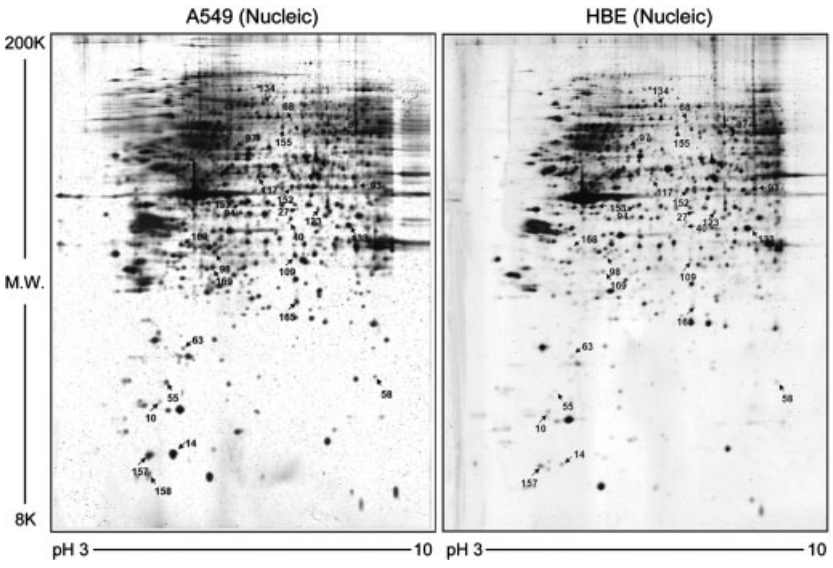

Figure 2. Representative 2-DE maps of nucleic proteins extracted from A549 and HBE cells. The identified proteins, as labeled by numbers on the gels, are listed in Supporting Information Table S1. Results were from one representative experiment out of three. Other representative 2-DE maps for whole-cell lysate and different subcellular fractions of A549 and HBE cells are shown in Supporting Information figures.

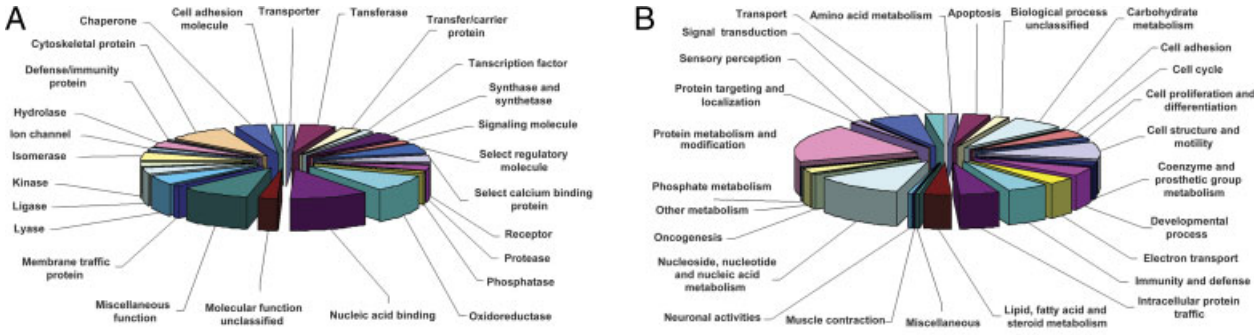

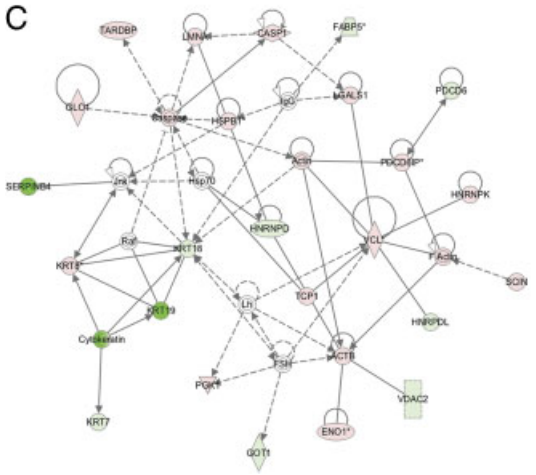

Figure 3. Functional annotation and pathway analysis. Pie chart representations of the distribution of identified DEPs according to their (A) molecular functions (B) biological processes. Categorizations were based on the information provided by the online resource PANTHER classification system. (C) Ingenuity Pathway Analysis. Pathway analysis was applied to global proteins and subcellular proteins by the ingenuity pathway. Shown is a graphical representation of the cellular assembly and organization. Abbreviations used are the same as in Supporting Information Table S1.

differential subcellular distribution of hnRNPK. Figure 5A shows a representative Western blotting result of hnRNPK expression in different fractions of A549 and HBE cells. Compared with that in HBE cells, hnRNPK has a significant upregulated expression in nucleus fraction in A549 cells. This expression pattern was identical to the protein level changes observed in 2-DE gels (Supporting Information Table S1). Similarly, immunocytochemistry results (Fig. 5B) showed the similar results of subcellular localization as obtained from Western blotting (Fig. 5A).

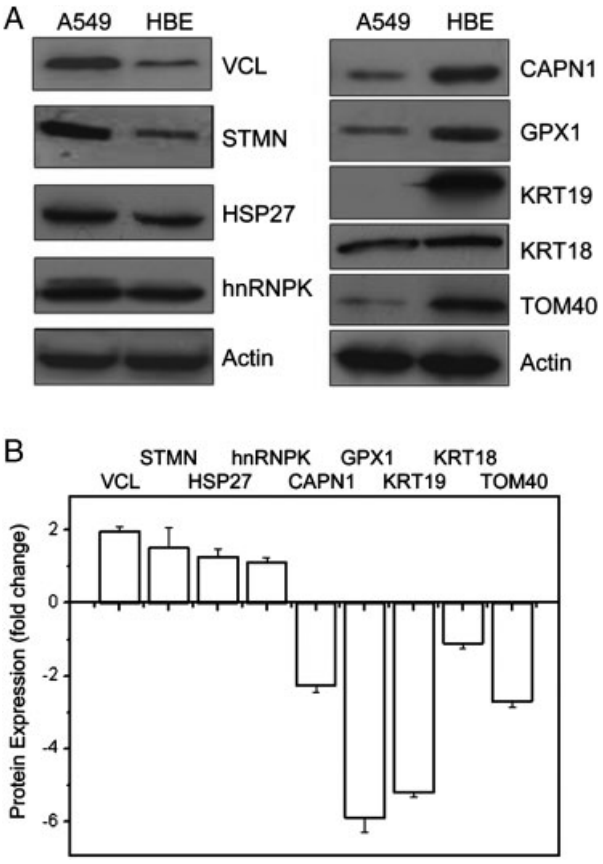

Figure 4. Western blotting images for nine proteins and loading control protein β-actin. (A) Western blotting showed changes in the expression levels of KRT18, KRT-19, HSP27, TOM40, hnRNPK, CAPN1, GPX1, stathmin, VCL between A549 and HBE cells. Experiment was conducted three times with similar results. The averaged fold changes with standard deviations are shown in (B).

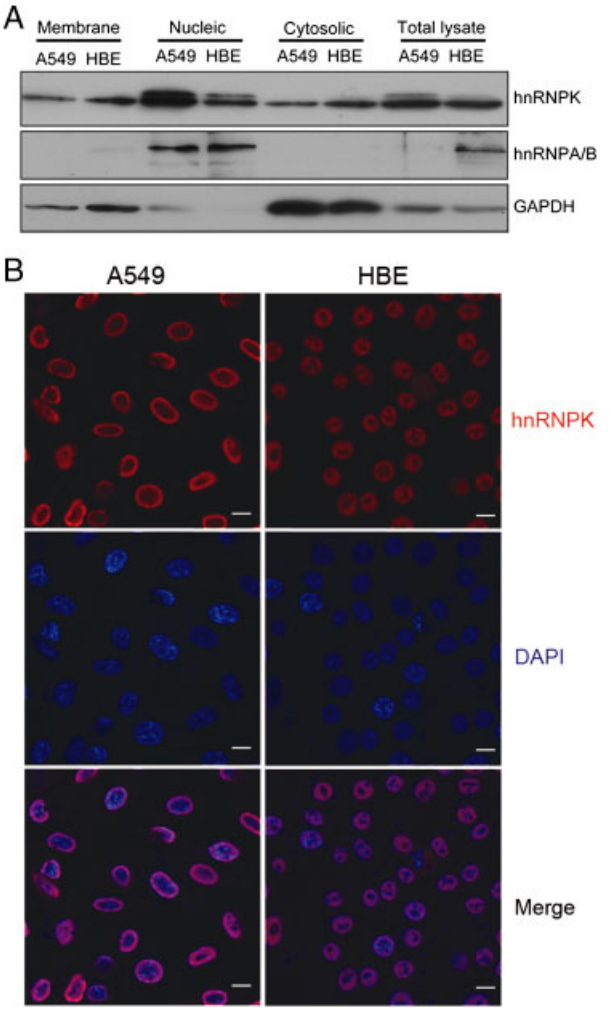

Figure 5. Subcellular localization of hnRNPK in A549 and HBE cells. (A) Western blotting analysis of hnRNPK expression in different fractions of the A549 and HBE cells. Compared with HBE cells, A549 cells had a marked upregulated expression of hnRNPK in nucleus. hnRNP A/B and GAPDH were used as internal controls for nucleic proteins and other fractions, respectively. (B) A549 and HBE cells were analyzed for the distribution of hnRNPK by immunocytochemistry. The cells were fixed and stained with anti-hnRNPK Ab followed by Texas red-conjugated secondary Ab (red signal). Nuclei were counter-stained with DAPI (blue signal). The results showed the nuclear accumulation of hnRNPK in A549 cells. Scale bar = 20μm.

3.6 EMT phenotype in A549 cells

In connection with the downregulation of KRT18 and KRT19, the two typical epithelial molecular markers [20], we further investigated whether EMT occurred in A549 cells. As shown in Fig. 6, the expression of epithelial markers, ZO-1, β-catenin, E-cadherin, KRT18, and KRT19 was significantly reduced in A549 cells comparing with that in HBE cells. On the contrary, mesenchymal markers, vimentin, and *N*-cadherin that positively correlated with EMT were dramatically upregulated in A549 cells, demonstrating that A549 cells may proceed a transition to an EMT phenotype.

3.7 TGF-β1 secretion in A549 cells

The pathway analysis indicated that A549 cells possessed more migration capacity and might undergo EMT transformation (Fig. 3). To correlate the pathway analysis with cell migration capacity, we posit TGF-β1 as a potential EMT inducer and tested the TGF-β1 concentration in the supernatants of the two cell lines. As shown in Fig. 7A, the supernatant concentration of TGF-β1 in A549 cultures was 229 ± 16 pg/mL, significantly higher than that in HBE cultures (9 ± 6 pg/mL) ($p < 0.01$, $n = 3$).

3.8 Silencing hnRNPK represses EMT phenotype in A549 cells

As suggested in the IPA network, hnRNPK can bind to VCL. We hypothesize that hnRNPK may function as a modulator

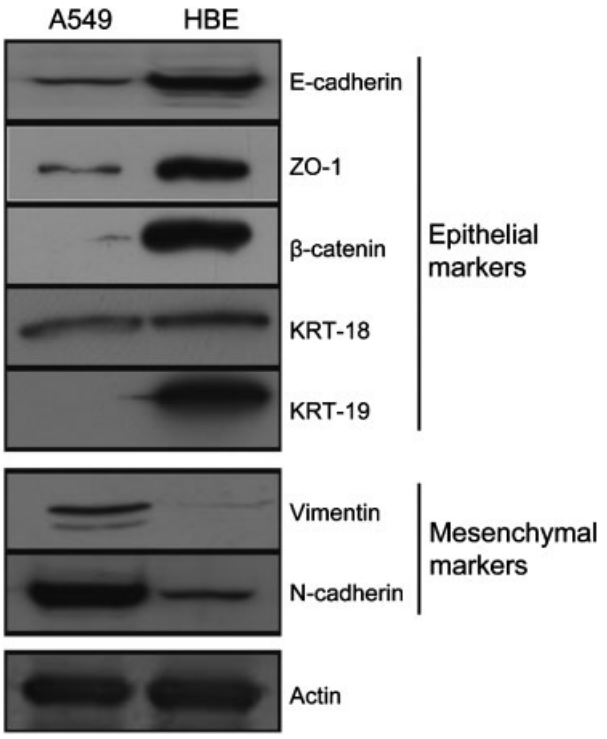

Figure 6. EMT phenotype biomarkers in A549 cells. Compared with HBE cells, A549 cells showed the expression inhibition of epithelial markers, E-cadherin, ZO-1, KRT18, KRT19, and β-catenin and the increases in the expression of mesenchymal markers, vimentin, and *N*-cadherin. β-Actin was used as a loading control.

of cell migration and thus affects the EMT phenotype of A549 cells. To test this hypothesis, we reduced the protein expression level of hnRNPK in A549 and HBE cells by RNA*i*, and then used TGF-β1 to induce EMT in A549 and HBE cells. Western blotting results showed that epithelial marker (E-cadherin) was downregulated, whereas mesenchymal marker (vimentin) was upregulated in A549 cells with TGF-β1 treatment (Fig. 7B), verifying that knockdown of hnRNPK repressed EMT phenotype in A549 cells.

These Western blotting results were then confirmed by immunocytochemistry, indicating higher level of vimentin and lower level of E-cadherin with the treatment of TGF-β1 in A549 cells (Fig. 7C). Similarly, pretreatment with siRNA for hnRNPK reduced these EMT phenotypes in A549 under the same conditions (Fig. 7C). E-cadherin is largely restricted to cell–cell interface in the parental cells of HBE cells; on the contrary, E-cadherin in A549 cells is mostly compartmentalized in cytoplasm and plasma membrane (Fig. 7C). Consistent with the immunoblotting assay, E-cadherin almost reached undetectable level after TGF-β1 stimulation for 24 h in A549 cells (Fig. 7C). However, the expression level of E-cadherin was greatly restored by knocking down hnRNPK (Fig. 7C). Similarly, the upregulation of vimentin under stimulation of TGF-β1 was also suppressed by the knockdown of hnRNPK (Fig. 7C). However, we did not observe the same phenomena in the parallel experiments with HBE cells (Fig. 7C).

As another EMT phenotype, F-actin polarization is known to be related to cell migration, cytoskeleton reassembly, and intracellular protein transportation [21]. A549 cells treated with TGF-β1 for 24 h can exhibit morphological change from the classical cobblestone appearance to the predominantly fibroblast-like cells (data not shown). Therefore, we posit that F-actin is an endpoint target of hnRNPK. Supportively, without interfering hnRNPK, we observed typical F-actin polarization in A549 cells upon TGF-β1 stimulation (Fig. 7D, arrowheads). However, this polarized F-actin distribution was remarkably reduced when knocking down hnRNPK (Fig. 7D). HBE cells largely did not respond to this EMT stimulation by TGF-β1, with F-actin being evenly distributed in all experimental groups (Fig. 7D).

4 Discussion

Subcellular proteomic technique employed in this study remarkably increased the efficiency of identifying fraction-specific proteins. This markedly facilitated subsequent pathway analysis and the reorganization of cellular migration associated with functional networks. Furthermore, regulation nodes of EMT transformation were discovered for downstream biological validations, leading to a better understanding of EMT mechanism in A549 cells. As a result, this study represents one of the first attempts to investigate lung cancer cell EMT in subcellular proteomic level.

In this study, IPA analysis suggested that proteomic differences between HBE and A549 cells were mechanistically relevant to the increased migration and EMT phenotype in the malignant cell line. Multiple proteins including VCL [22, 23], PDCD6IP [24], and HSBP [25–27] in the network detected by IPA have been reported to be directly related to F-actin polarization and cytoskeleton reassembly. Based on these observations, together with the downregulation of KRT18 and KRT19 in A549 cells, we can speculate that A549 cells have an EMT phenotype. Other groups have also demonstrated that the downregulation of KRT18 and KRT19 is one of the hallmark molecular changes occurred during EMT [20, 28–30].

We further provided evidences to support the EMT phenotype shift of A549 cells, including the downregulation of E-cadherin, β-catenin, Snail, and ZEB, and the up-regulation of vimentin and *N*-cadherin. These changes in protein expression indicated the loss of cell–cell adhesion (downregulation of E-cadherin), enhanced matrix degradation ability (proteases overproduction), increased activation level (upregulated vimentin and *N*-cadherin), and transcription factor alterations (β-catenin, Snail, ZEB, and basic helix-loop-helix families) [31]. These molecular events are often modulated by one of the classic signaling pathways including WNT, TGF-β, Hedgehog, Notch, and receptor tyrosine

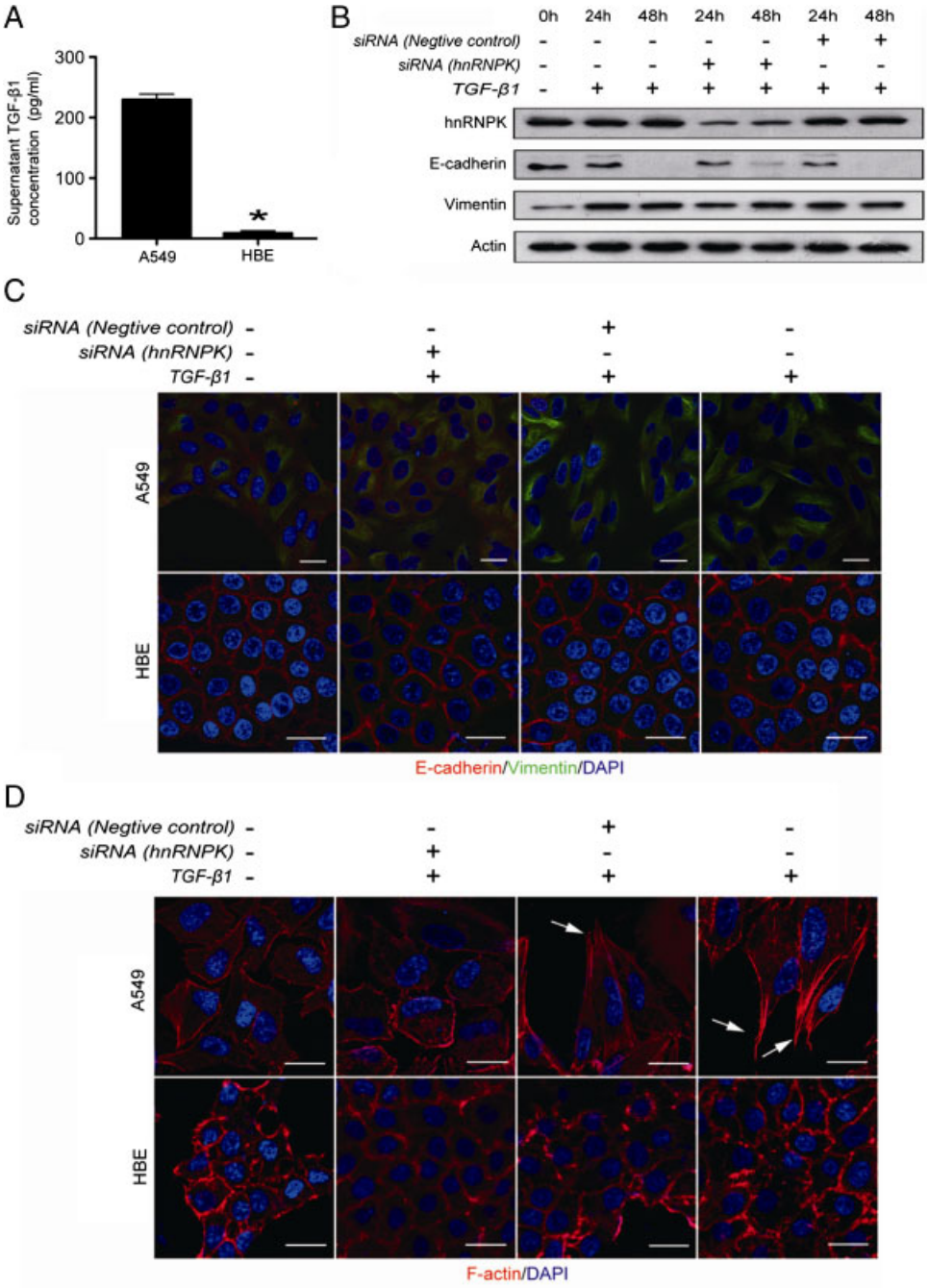

Figure 7. TGF-β1-mediated EMT phenotype can be inhibited by knocking down hnRNPK. (A) Supernatant TGF-β1 secretion level in A549 and HBE cells detected by ELISA. The same number of A549 and HBE cells was incubated for 20 h using DMEM without FBS. Data shown were described as mean ± SD (*$p < 0.01$, $n = 3$). (B) Western blotting analysis of hnRNPK involved in EMT. A549 cells were treated with hnRNPK siRNA for 24 h, and then subjected to serum deprivation for 24 h before being stimulated with 5 ng/mL TGF-β1. (C) Immunofluorescent analysis for EMT markers. Immunofluorescent staining for E-cadherin and vimentin in A549 and HBE cells. E-cadherin (red), vimentin (green), and DAPI (blue) staining was shown, respectively. Scale bar = 20 μm. (D) F-actin polarization. A549 and HBE cells were stained with F-actin (red) and DAPI (blue). Arrowheads polarized distribution of intracellular F-actin. TGF-β1 was used at 5 ng/mL for 24 h treatment. Scale bar = 20 μm.

kinase that are frequently dysregulated in cancer and have been shown to stimulate EMT [31]. In addition, we showed that A549 cells produce more TGF-β1 than HBE cells, and that A549 displayed increased migratory phenotype in response to TGF-β1 stimulation. It is likely that self-secreting factors from A549 cells may in turn promote their own EMT, suggesting a possible mechanism in which malignant cells may produce EMT relevant factors to increase population migration ability, thus gaining more invasive and metastatic potential.

Interestingly, IPA also suggested that hnRNPs are positive regulation nodes in the migration-related network. Three RNPs, hnRNP D-like, K, and C were identified in the present study. hnRNPs are a group of RNA-binding proteins in intranucleus of eukaryon cells. They bind pre-mRNA in a sequence-specific manner and determine whether and how a specific mRNA ends its journey in splicing and processing [32]. Another important function of hnRNPs, especially hnRNPK in benign MCR5 cells, is to modulate cell-matrix attachment via acting on RNA and RNA-binding proteins, a

critical modulation for cell spreading and migration [33]. Although hnRNPK and VCL colocalization was observed upon cell spreading [33], which is consistent with IPA network computed in this study, the mechanism of how hnRNPK-VCL binding acts on cell migration is largely unknown.

We demonstrated direct connection of hnRNPK upregulation in A549 cells with increased ability of cellular migration and EMT. Upon TGF-β1 stimulation, A549 cells showed polarized F-actin distribution that is a typical migratory phenotype; however, this polarization can be blocked by hnRNPK knockdown. Consistently, increased EMT was observed by analyzing relevant protein markers, such as E-cadherin and vimentin. Several reports implicated that hnRNPK have a role in tumor development and progression [34]. For instance, hnRNPK contributes toward multiple myeloma by binding the mutant mRNA strand increasing translation of the oncogene *c*-myc [35] and hnRNPK expression is regulated by the p53/MDM 2 pathway [36]. The overexpression of hnRNPK found in this study was supported by the observations of hnRNPK upregulation in several different cancer types inclusive of lung and liver cancers [37, 38], reinforcing its important role in carcinogenesis.

The differentially expressed initiation and elongation factors identified in this study (Supporting Information Table S1 and Fig. 2) implicated their relevance to carcinogenesis. Especially, it has been widely reported that the overexpression of eIF4 is one of the prevalent mechanisms underlying the selective upregulation of metastasis-associated gene transcription, thus positively relevant to numerous malignancies [39, 40]. Comparable phenomena exited in the context of the eIF5A2-induced upregulation of cancer cell migratory phenotypes [41, 42]. These clues indicate a potentially regulatory effect of initiation and elongation factors on the increased migration ability of A549 cells.

The identified 15 cytoskeletal proteins contain seven intermediate filament proteins, including three lamins and three keratins. Intermediate filaments are abundant cytoplasmic and nuclear proteins that can be classified into five groups based on the domain and sequence homology [43]. Especially, the downregulation of keratins and the upregulation of vimentin in A549 cells detected in this study are interesting phenomena. Studies in other groups also found that major keratins loss and their replacement with vimentin occur during EMT transformation, indicating potential correlations between cytoskeletal protein rearrangement and malignant metastasis [28, 44].

In addition, we identified the upregulation of 26S proteasome subunits in nucleus fraction, including proteasome subunit α type-3 (PSMA3) and proteasome subunit β type-3 (PSMB3). Ubiquitin–proteasome system is crucial for degrading unfolded proteins and other substrates, and therefore relevant to proliferation regulation, anti-viral responses as well as numerous neurodegenerative, metabolic, and cardiovascular diseases. In cancer cells, it has been reported that PI3K pathway can activate the phosphorylation of ubiquitin E3 ligases HDM2 involved in p53 degradation, thus inhibiting p53-mediated apoptosis [45].

Based on our results and findings of other groups mentioned above, we summarized the potential mechanisms of EMT in A549 cells (Fig. 8). The process of EMT in A549 may activate PI3 kinase pathway through the phosphorylation of AKT and then HDM2. The phosphorylated HMD2 can translocate to the nucleus to take part in the decay of the cancer suppressor gene *p53* and the activation of oncogene regulator hnRNPK and KHSRP. Targeting critical orchestrators at the convergence of several EMT signaling pathways, such as the AKT/mTOR axis and the NF-κB, MAPK, PKC, β-catenins, and AP-1/SMAD EMT transcription pathways, may provide a realistic strategy to control EMT and the progression of human epithelial cancers [46–48]. Indeed, several pharmaceutical companies have already engaged in preclinical research and clinical trials with new generation of therapeutic small molecules targeting these orchestrators in epithelial tumors [49]. On the other hand, since some proteins known to induce EMT seem to be markers of carcinoma progression, EMT could be a valid approach in identifying new molecules whose expression is associated with adverse prognostic factors [50, 51]. Therefore, our findings of the EMT phenotype in lung cancer cells provide insights for understanding the pathogenesis of lung cancer, and also suggest potential therapeutic strategies for the treatment of lung cancer.

In conclusion, subcellular proteomic approach was employed to compare the protein profiles between A549 and HBE cells for the first time. Many proteins with differential expression were confidentially identified and interesting clues for lung carcinogenesis were derived based on the protein characteristics. Especially, our in-depth functional

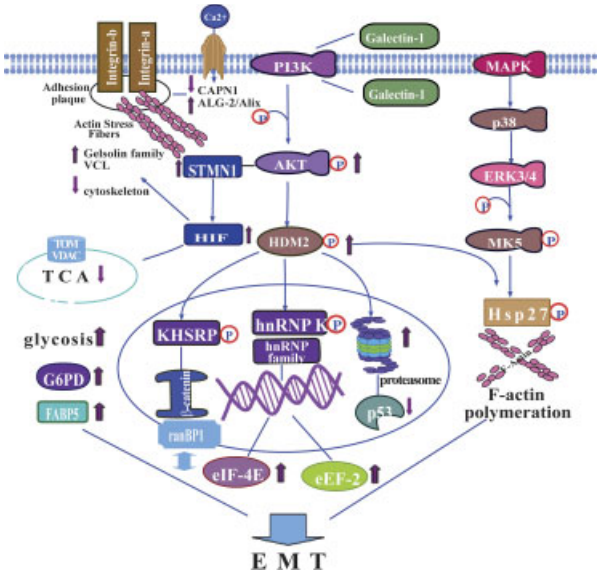

Figure 8. Schematic diagram showing possible mechanisms of EMT involved in A549 cells.

analyses indicated that EMT phenotype occurs in A549 cells and that hnRNPK could be a therapeutic target for containing the invasiveness of lung cancer cells. These novel findings provide mechanistic insights into lung carcinogenesis and will benefit the identification of potential drug targets for lung cancer treatment.

This work was partially supported by the 2007 Chang-Jiang Scholars Program, "211" Projects, National Basic Research Program of China (973 Program). The Fundamental Research Funds for the Central Universities, Open Funds from the State Key Laboratory of Respiratory Disease, the Science and Technology Planning Projects of Guangzhou and Guangdong, China.

The authors have declared no conflict of interest.

5 References

[1] Jemal, A., Siegel, R., Ward, E., Murray, T. et al., Cancer statistics, 2006. *CA-A Cancer J. Clin.* 2006, *56*, 106–130.

[2] Chen, G. A., Gharib, T. G., Wang, H., Huang, C. C. et al., Protein profiles associated with survival in lung adenocarcinoma. *Proc. Natl Acad. Sci. USA* 2003, *100*, 13537–13542.

[3] Morio, A., Miyamoto, H., Izumi, H., Risk of recurrence after surgical resection of small-sized invasive lung adenocarcinoma: analysis based on apoptotic index. *Jpn. J. Thorac. Cardiovasc. Surg.* 2005, *53*, 345–353.

[4] Geho, D. H., Bandle, R. W., Clair, T., Liotta, L. A., Physiological mechanisms of tumor-cell invasion and migration. *Physiology* 2005, *20*, 194–200.

[5] Christiansen, J. J., Rajasekaran, A. K., Reassessing epithelial to mesenchymal transition as a prerequisite for carcinoma invasion and metastasis. *Cancer Res.* 2006, *66*, 8319–8326.

[6] Thiery, J. P., Epithelial-mesenchymal transitions in tumour progression. *Nat. Rev. Cancer* 2002, *2*, 442–454.

[7] Berx, G., Raspe, E., Christofori, G., Thiery, J. P., Sleeman, J. P., Pre-EMTing metastasis? Recapitulation of morphogenetic processes in cancer. *Clin. Exp. Metastasis* 2007, *24*, 587–597.

[8] Hugo, H., Ackland, M. L., Blick, T., Lawrence, M. G. et al., Epithelial-mesenchymal and mesenchymal – epithelial transitions in carcinoma progression. *J. Cell. Physiol.* 2007, *213*, 374–383.

[9] Kokkinos, M. I., Wafai, R., Wong, M. K., Newgreen, D. F. et al., Vimentin and epithelial-mesenchymal transition in human breast cancer – observations in vitro and in vivo. *Cells Tissues Organs* 2007, *185*, 191–203.

[10] Lawrence, M. G., Veveris-Lowe, T. L., Whitbread, A. K., Nicol, D. L., Clements, J. A., Epithelial-mesenchymal transition in prostate cancer and the potential role of kallikrein serine proteases. *Cells Tissues Organs* 2007, *185*, 111–115.

[11] Katoh, M., Epithelial-mesenchymal transition in gastric cancer (Review). *Int. J. Oncol.* 2005, *27*, 1677–1683.

[12] Rho, J. K., Choi, Y. J., Lee, J. K., Ryoo, B. Y. et al., Epithelial to mesenchymal transition derived from repeated exposure to gefitinib determines the sensitivity to EGFR inhibitors in A549, a non-small cell lung cancer cell line. *Lung Cancer* 2009, *63*, 219–226.

[13] Thomson, S., Buck, E., Petti, F., Griffin, G. et al., Epithelial to mesenchymal transition is a determinant of sensitivity of non-small-cell lung carcinoma cell lines and xenografts to epidermal growth factor receptor inhibition. *Cancer Res.* 2005, *65*, 9455–9462.

[14] Ge, F., Lu, X. P., Zeng, H. L., He, Q. Y. et al., Proteomic and functional analyses reveal a dual molecular mechanism underlying arsenic-induced apoptosis in human multiple myeloma cells. *J. Proteome Res.* 2009, *8*, 3006–3019.

[15] Lei, T., He, Q. Y., Cai, Z., Zhou, Y. et al., Proteomic analysis of chromium cytotoxicity in cultured rat lung epithelial cells. *Proteomics* 2008, *8*, 2420–2429.

[16] Thomas, P. D., Campbell, M. J., Kejariwal, A., Mi, H. Y. et al., PANTHER: a library of protein families and subfamilies indexed by function. *Genome Res.* 2003, *13*, 2129–2141.

[17] Mi, H. Y., Guo, N., Kejariwal, A., Thomas, P. D., PANTHER version 6: protein sequence and function evolution data with expanded representation of biological pathways. *Nucleic Acids Res.* 2007, *35*, D247–D252.

[18] Wang, T., Gong, N., Liu, J., Kadiu, I. et al., Proteomic modeling for HIV-1 infected microglia-astrocyte crosstalk. *PloS ONE* 2008, *3*, e2507.

[19] Wang, T., Gong, N., Liu, J., Kadiu, I. et al., HIV-1-infected astrocytes and the microglial proteome. *J. Neuroimmune Pharmacol.* 2008, *3*, 173–186.

[20] Willipinski-Stapelfeldt, B., Riethdorf, S., Assmann, V., Woelfle, U. et al., Changes in cytoskeletal protein composition indicative of an epithelial-mesenchymal transition in human micrometastatic and primary breast carcinoma cells. *Clin. Cancer Res.* 2005, *11*, 8006–8014.

[21] Insall, R. H., Machesky, L. M., Actin dynamics at the leading edge: from simple machinery to complex networks. *Dev. Cell* 2009, *17*, 310–322.

[22] Wen, K. K., Rubenstein, P. A., DeMali, K. A., Vinculin nucleates actin polymerization and modifies actin filament structure. *J. Biol. Chem.* 2009, *284*, 30463–30473.

[23] DeMali, K. A., Barlow, C. A., Burridge, K., Recruitment of the Arp2/3 complex to vinculin: coupling membrane protrusion to matrix adhesion. *J. Cell Biol.* 2002, *159*, 881–891.

[24] Pan, S., Wang, R., Zhou, X., He, G. et al., Involvement of the conserved adaptor protein Alix in actin cytoskeleton assembly. *J. Biol. Chem.* 2006, *281*, 34640–34650.

[25] Lavoie, J. N., Hickey, E., Weber, L. A., Landry, J., Modulation of actin microfilament dynamics and fluid phase pinocytosis by phosphorylation of heat shock protein 27. *J. Biol. Chem.* 1993, *268*, 24210–24214.

[26] Rust, W., Kingsley, K., Petnicki, T., Padmanabhan, S. et al., Heat shock protein 27 plays two distinct roles in controlling

human breast cancer cell migration on laminin-5. *Mol. Cell. Biol. Res. Commun.* 1999, *1*, 196–202.

[27] Guo, K., Liu, Y., Zhou, H., Dai, Z. et al., Involvement of protein kinase C beta-extracellular signal-regulating kinase 1/2/p38 mitogen-activated protein kinase-heat shock protein 27 activation in hepatocellular carcinoma cell motility and invasion. *Cancer Sci.* 2008, *99*, 486–496.

[28] Paccione, R. J., Miyazaki, H., Patel, V., Waseem, A. et al., Keratin down-regulation in vimentin-positive cancer cells is reversible by vimentin RNA interference, which inhibits growth and motility. *Mol. Cancer Ther.* 2008, *7*, 2894–2903.

[29] Mathias, R. A., Simpson, R. J., Towards understanding epithelial-mesenchymal transition: a proteomics perspective. *Biochim. Biophys. Acta Proteins Proteomics* 2009, *1794*, 1325–1331.

[30] Moll, R., Divo, M., Langbein, L., The human keratins: biology and pathology. *Histochem. Cell Biol.* 2008, *129*, 705–733.

[31] Thiery, J. P., Sleeman, J. P., Complex networks orchestrate epithelial-mesenchymal transitions. *Nat. Rev. Mol. Cell Biol.* 2006, *7*, 131–142.

[32] Bomsztyk, K., Denisenko, O., Ostrowski, J., HnRNP K: one protein multiple processes. *Bioessays* 2004, *26*, 629–638.

[33] de Hoog, C. L., Foster, L. J., Mann, M., RNA and RNA binding proteins participate in early stages of cell spreading through spreading initiation centers. *Cell* 2004, *117*, 649–662.

[34] Mukhopadhyay, N. K., Kim, J., Cinar, B., Ramachandran, A. et al., Heterogeneous nuclear ribonucleoprotein K is a novel regulator of androgen receptor translation. *Cancer Res.* 2009, *69*, 2210–2218.

[35] Evans, J. R., Mitchell, S. A., Spriggs, K. A., Ostrowski, J. et al., Members of the poly (rC) binding protein family stimulate the activity of the c-myc internal ribosome entry segment in vitro and in vivo. *Oncogene* 2003, *22*, 8012–8020.

[36] Moumen, A., Masterson, P., O'Connor, M. J., Jackson, S. P., hnRNP K: an HDM2 target and transcriptional coactivator of p53 in response to DNA damage. *Cell* 2005, *123*, 1065–1078.

[37] Pino, I., Pio, R., Toledo, G., Zabalegui, N. et al., Altered patterns of expression of members of the heterogeneous nuclear ribonucleoprotein (hnRNP) family in lung cancer. *Lung Cancer* 2003, *41*, 131–143.

[38] Ostrowski, J., Bomsztyk, K., Nuclear shift of hnRNP K protein in neoplasms and other states of enhanced cell proliferation. *Br. J. Cancer* 2003, *89*, 1493–1501.

[39] De Benedetti, A., Graff, J. R., eIF-4E expression and its role in malignancies and metastases. *Oncogene* 2004, *23*, 3189–3199.

[40] Graff, J. R., Zimmer, S. G., Translational control and metastatic progression: enhanced activity of the mRNA cap-binding protein eIF-4E selectively enhances translation of metastasis-related mRNAs. *Clin. Exp. Metastasis* 2003, *20*, 265–273.

[41] Tang, D. J., Dong, S. S., Ma, N. F., Xie, D. et al., Overexpression of eukaryotic initiation factor 5A2 enhances cell motility and promotes tumor metastasis in hepatocellular carcinoma. *Hepatology* , 51, 1255–1263.

[42] Xie, D., Ma, N. F., Pan, Z. Z., Wu, H. X. et al., Overexpression of EIF-5A2 is associated with metastasis of human colorectal carcinoma. *Hum. Pathol.* 2008, *39*, 80–86.

[43] Hesse, M., Magin, T. M., Weber, K., Genes for intermediate filament proteins and the draft sequence of the human genome: novel keratin genes and a surprisingly high number of pseudogenes related to keratin genes 8 and 18. *J. Cell Sci.* 2001, *114*, 2569–2575.

[44] Crowe, D. L., Milo, G. E., Shuler, C. F., Keratin 19 down-regulation by oral squamous cell carcinoma lines increases invasive potential. *J. Dent. Res.* 1999, *78*, 1256–1263.

[45] Brooks, C. L., Gu, W., p53 ubiquitination: Mdm2 and beyond. *Mol. Cell* 2006, *21*, 307–315.

[46] Faivre, S., Kroemer, G., Raymond, E., Current development of mTOR inhibitors as anticancer agents. *Nat. Rev. Drug Discov.* 2006, *5*, 671–688.

[47] LoPiccolo, J., Blumenthal, G. M., Bernstein, W. B., Dennis, P. A., Targeting the PI3K/Akt/mTOR pathway: effective combinations and clinical considerations. *Drug Resist. Updat.* 2008, *11*, 32–50.

[48] Peinado, H., Cano, A., New potential therapeutic targets to combat epithelial tumor invasion. *Clin. Transl. Oncol.* 2006, *8*, 851–857.

[49] Broxterman, H. J., Georgopapadakou, N. H., Anticancer therapeutics: a surge of new developments increasingly target tumor and stroma. *Drug Resist. Updat.* 2007, *10*, 182–193.

[50] Bellovin, D. I., Simpson, K. J., Danilov, T., Maynard, E. et al., Reciprocal regulation of RhoA and RhoC characterizes the EMT and identifies RhoC as a prognostic marker of colon carcinoma. *Oncogene* 2006, *25*, 6959–6967.

[51] Spaderna, S., Schmalhofer, O., Hlubek, F., Berx, G. et al., A transient, EMT-linked loss of basement membranes indicates metastasis and poor survival in colorectal cancer. *Gastroenterology* 2006, *131*, 830–840.

